D 3719

Materialwissenschaft und Werkstofftechnik

Materials Science and Engineering Technology

11/2008

Titelbild: Carbide Net

Nanophase hardfaced coatings

Osseointegration of a novel, hydropholic Ti surface

Dehnungswöhlerlinie und Spannungs-Dehnungs-Kurve

FEM analysis of pseudoelastic NiTi shape memory alloys

Carbonated hydroxyapatite nanopowders

Co-extruded wear resistant powder metallurgical layers

Chelating fibrous polymer by different diamines

Laser welding of stainless steel

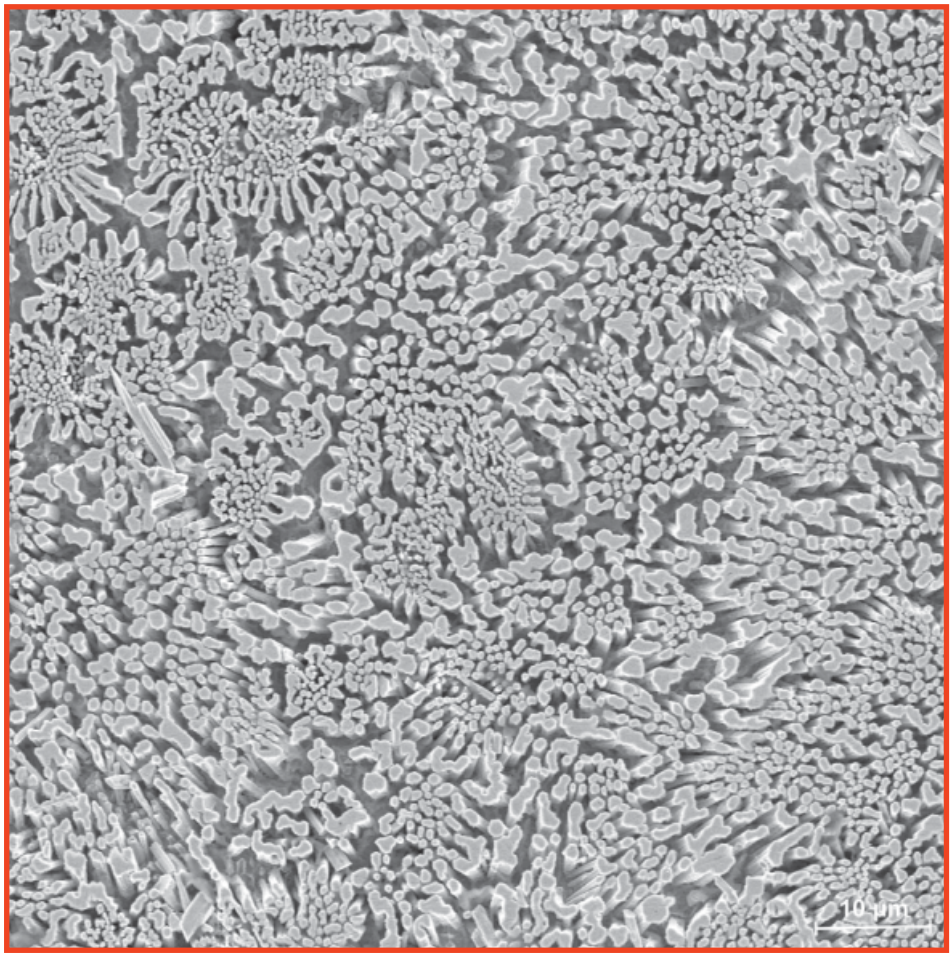

WILEY-VCH

Reprint

MATWER 39 (11) 787–854 (2008) · ISSN 0933-5137
Vol. 39 – No. 11 – November 2008

Carbonated hydroxyapatite nanopowders for preparation of bioresorbable materials

E. S. Kovaleva[1], M. P. Shabanov[2], V. I. Putlayev[1], Ya. Yu. Filippov[1], Y. D. Tretyakov[1], V. K. Ivanov[3]

Incorporation of carbonate ions to the crystal structure of carbonated hydroxyapatite (CHAp) leads to the formation of point defects (vacancies) in Ca- and OH-sublattices as well as to microstrains revealed in CHAp nanocrystals. Various techniques, such as XRD, FTIR, TEM, FESEM/EDX, TG/DTA, AES (ICP), wet chemical analysis, Ca-ionometry, microvolumetric analysis of evolved CO_2, BET adsorption, were applied to determine an efficiency of carbonate substitution, and to quantify the elemental composition, as well as to characterize the structure of the carbonated hydroxyapatite and the site(s) of carbonate substitution. It was shown that there is insignificant incorporation of Na into the crystal structure of HAp. Over the range of 0–4 % wt. ($x<0.25$), the substitution of OH- by CO_3^{2-} takes place leading to A-Type of CHAp, further increase of CO_3^{2-}-content enhances PO_4^{3-}-substitution giving AB-type of CHAp. According to *in vitro* test, the bioactivity of the samples is increasing with the growth of carbonate content due to accumulation of the defects in CHAp nanocrystals.

Key words: Carbonated hydroxyapatite; Aliovalent doping; Point defects; Microstrains; Real structure; Resorption.

1 Introduction

Ceramics and composites based on calcium phosphates are known to be prospective materials for making bone implants to substitute damage or deceased parts of bones. Noticeable attention is paid to hydroxyapatite $Ca_{10}(PO_4)_6(OH)_2$ (HAp) due to its affinity to a bone mineral [1,2]. Meanwhile, human bone mineral differs in composition from stoichometric HAp in that it contains additional ions, of which carbonate is the most abundant specie (*ca.* 8 wt.%) [3,4]. Pure HAp has some disadvantages compared to biogenic apatite, particularly, its resorption *in vivo*, too sluggish to induce a massive formation of a new bone tissue, is considered as a serious drawback. Possible way to enhance biological properties of an implant passes through the chemical modification of HAp. [2]. It is known that incorporation of carbonate ions has considerable impact on stability of crystal lattice and, hence, on mineralization, demineralization, remineralization processes [1,3]. Introduction of carbonate ions in HAp would, thus, increase its dissolution rate in solution and could enhance its osteointegration rate [1,5]. Coming from this viewpoint, it is widely accepted that carbonated hydroxyapatite is a prospective material for medicine in order to mimic the composition of native bone. It is more soluble and bioactive material than stoichiometric HAp [1,2,5].

Carbonate ion, assuming its effective ionic radius and its basic properties (*i.e.* its affinity to anionic sites in HAp lattice), is situated right in between PO_4^{3-} and OH^- ions. Evidently, carbonate ion can substitute at two sites in the apatite structure, namely, the hydroxyl and the phosphate ion position, giving rise to A- and B-type carbonated hydroxyapatite (CHAp), respectively [3,4,6]. Preference of CO_3^{2-} to substitute at a certain site might be determined by conditions of CHAp synthesis. In addition, sodium ions, either found in bone, are also known to increase the maximum ratio of carbonate substitution in B-site, because its incorporation in calcium sites induces a favorable electrical charge balance [6]. The role of carbonate on biological behavior of pure single phased carbonated hydroxyapatites without alkali remains unclear.

In real structure of CHAp crystal two types of defects have to play an important role: free surface (since the size of CHAp nanocrystals precipitated from solutions are usually less than 100 nm) and local distortions of the lattice leading to a complex strain pattern (since the ionic radius of carbonate ion is less than that of phosphate ion by 30 %). The latter can cause inhomogeneous distribution of the dopant across the crystal, namely, in the vicinity of crystal surface. Such a distribution drastically affects acid-base properties of the apatite surface and, therefore, the initial rate of dissolution of the crystal. It is particularly important for an active (fast) phase of resorption taking place in acidic media under the action of osteoclasts. In the case of sluggish phase of resorption spontaneously developing in solutions at near physiological values of pH, stability of the CHAp lattice (which, in fact, decreases with the growth of carbonate content, assuming, largely, substitution of the B-type) is of importance. It is not evident how the change of substitution mechanism, situated as CO_3^{2-} content grows, will affect the real structure of CHAp crystal, further, its solubility, and, finally, its behavior *in vitro* and *in vivo*. Therefore, it is of fundamental importance to know the mechanism for carbonate incorporation in hydroxyapatite. Carbonated hydroxyapatite with varied and controlled amounts of carbonate ions in A and B-sites of the apatite structure has never been under extended study aimed at evaluation of the sequence: carbonate content – microsructure – resorption *in vitro* [1,6,7]. The purpose of this work was to find and investigate a correlation between the carbonate ion content in crystalline lattice and defect structure, and solubility of the materials; finally, to prepare the materials under study for *in vitro* and *in vivo* tests

[1] Department of Materials Science, Moscow State University, Moscow, Russia

[2] Department of Chemistry, Moscow State University, Moscow, Russia

[3] Kurnakov's Institute of General and Inorganic Chemistry of RAS, Moscow, Russia

2 Experimental Part

2.1 Materials preparation

Carbonated hydroxyapatite nanopowders with various degrees of carbonate substitution were prepared by an aqueous precipitation method according to the following equation:

$$(10\text{-}x)\ Ca(NO_3)_2 + (6\text{-}x)\ (NH_4)_2HPO_4 + x\ Na_2CO_3 + (8\text{-}x)\ NH_4OH \rightarrow Ca_{10\text{-}x}Na_x(PO_4)_{6\text{-}x}\ (CO_3)_x(OH)_2 + (20-3x)\ NH_4NO_3 + x\ NaNO_3 + (6\text{-}x)\ H_2O,$$

where x = 0, 0.25, 0.5, 0.75, 1, 1.5, 2, by drop-wise addition of 0.3 M stock solution of ammonium phosphate $(NH_4)_2HPO_4$, 99.9 %, Labteh, Russia) with appropriate amount of sodium hydrogencarbonate ($NaHCO_3$, 99.9 %, Labteh, Russia) to 0.5 M stock solution of calcium nitrate ($Ca(NO_3)_2{\cdot}4H_2O$, 99.9 %, Labteh, Russia). Prior to making the stock solutions all the reagents were checked for the content of main substances by gravimetric or titrimetric chemical analyses. The pH value of the stock solutions was pre-adjusted at 11.5 by addition of NH_4OH (30 wt.%), and then it was maintained manually at the constant value of 12.0 ($\pm$0.5) by addition of the concentrated solution of ammonium hydroxide. The pH-meter Expert-001 (Econix, Russia) with glass electrode ESK-1030 (Russia) was used to monitor pH value. The temperature was controlled and regulated at 80 $\pm$ 1 °C. After total mixing of the stock solutions, the suspension was ripened and heated using a thermostatically controlled hot plate for 24 hours under constant stirring. Then, a precipitate was filtered and washed with 300 mL of distilled water. The resulting precipitate was dried at room temperature in air. Dry powders were heat treated for 1 hour at 260 °C in air in order to reach better crystallinity and to eliminate the adsorbed moisture and the synthesis residues such as nitrous species. It was concluded that this thermal treatment did not affect the structure of the precipitates since the lattice parameters change slightly (less then 0.005 Å), there were no any differences in IR spectra, and Ca/P ratio remained unchanged.

2.2 Materials characterization

The as-received and heat treated powders were studied by X-ray diffraction analysis in the interval of angles 2Θ= 10–110° (Cu Kα radiation, Rigaku D/MAX 2500 with rotating anode, Japan) and IR spectroscopy in 400–4000 cm^{-1} range (pellets: 1 mg of powder in 150 mg of analytical grade KBr, Ø = 13 mm, Perkin-Elmer 1600 FTIR spectrophotometer, USA). Sizes of crystallites and microstrain parameters were extracted from X-ray diffraction line profile using Scherrer- and Wilson-formulas from Williamson-Hall-plots according to the procedure of de Keijser, Langford, Mittemeijer *et al*. [8] with the help of STOE WinXPOW software (STOE&Cie GmbH, Germany).

The micromorphology of the powders was examined by scanning and transmission electron microscopy (JEM-2000FX II, JEOL, Japan, operated at 200 kV; and FESEM LEO SUPRA 50VP, Carl Zeiss, Germany, 5 kV).

The Ca-content of the CHA precipitates was quantified by EDTA titration. Phosphorous content was determined using the quinolinium phosphomolybdate method modified by Dahlgren [9]. The content of Na was determined using AES (ICP) with Optima 5300DV (Perkin-Elmer, USA). In some cases Ca/P ratio of the CHA samples was obtained independently from EDX data (INCA Energy+, Oxford Instruments, UK, attached to LEO SUPRA 50 VP). The carbonate content was analyzed with microvolumetric determination of CO_2 released from the samples under their dissolution in nitric acid. The overall content of CO_2 and H_2O was examined by TG/DTA (Diamond Pyris, Perkin Elmer, USA, quasi-isothermal heating to maintain decomposition rate at 10 µg/min; STA 409 PC, Netzsch, Germany, with IR-analysis of evolved gases). The specific surface area of each carbonated hydroxyapatite was determined by BET method with nitrogen as adsorbate (Nova 4200e, Quantachrome, USA).

Bioactivity of the CHA samples was assessed *in vitro* using experiments on dissolution (resorption) of the samples in acidic media and precipitation of apatite layer on the surface of the samples from supersaturated solutions under physiological pH. Dissolution rate of CHA samples was studied by measuring pCa (pH-meter-ionomer Expert-001, Econix, Russia, computer acquiring of signal with a discrete of 1 s) of 0.1 g of the sample in 100 ml of 0.1 M acetic buffer (pH=5.5) at 37 °C for up to 24 hrs. Specific dissolution rate w ($m^2{\cdot}g^{-1}{\cdot}s$) was calculated as

$$w = \frac{d(\mathrm{pCa})/dt|_{t=0}}{(\mathrm{pCa}_0 - \mathrm{pCa}_\infty)\cdot s}$$

from experimental curves pCa=$f(t)$, where pCa_0 is the initial value of pCa (at t=0), and pCa_∞ is the asymptotic value at end of experiment, s is specific surface of the sample ($m^2{\cdot}g^{-1}$). In precipitation experiments SBF media was used (Simulated Body Fluid: 142 mM Na^{+}, 5 mM K^{+}, 1.5 mM Mg^{2+}, 2.5 mM Ca^{2+}, 147.8 mM Cl^{-}, 27 mM HCO_3^{-}, 1 mM HPO_4^{2-}, SO_4^{2-}, tris-buffer). SBF was prepared in accordance with a chemical composition of human body fluid, with ion concentrations nearly equal to those of the inorganic constituents of human blood plasma, following Kokubo *et al* [10]. Pelletized samples were soaked in SBF for different time intervals (from 7 to 21 days) at 37 °C and pH 7.4. Afterward, they were examined with SEM to analyze a fresh apatite layer precipitated from SBF.

Long-term co-culturing of human fibroblasts with the CHAp materials *in vitro* was done in DMEM/F12 cultural media with addition of growth factors, glutamine, and 10 % of serum at 37 °C, humidity of 97 %, 5 % of CO_2 in a cultural box up to three weeks. Afterward, cultured samples were stained with FITC, PI, and Hoechst 33342. Fluorescent images were captured with the help of inverted microscope Axsiovert 25 equipped with mbq 52 ac and DP 500 color camera.

3 Results and Discussion

X-ray diffraction (XRD) analysis showed the diffraction patterns that correspond to those of HAp (# 9–432 from ICDD PDF-2) for all samples (*Fig.1*). The as-received powders were found to be nanocrystalline as it was evidenced from broad diffraction peaks, and free of secondary phases. An increase of carbonate content is associated with decreasing in crystallite sizes in agreement with Gibson *et al* [3]. The carbonate substitutions in hydroxyapatites are known to change the crystal lattice parameters. It is widely accepted that a pure type A causes extension of the *a*- and contraction of the *c*-axis parameters, in contrast, a pure type B carbonated apatite de-

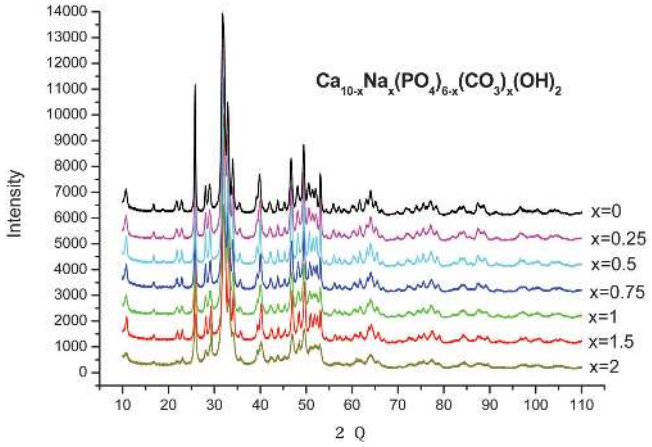

Figure 1. XRD patterns of CHAp with various x.

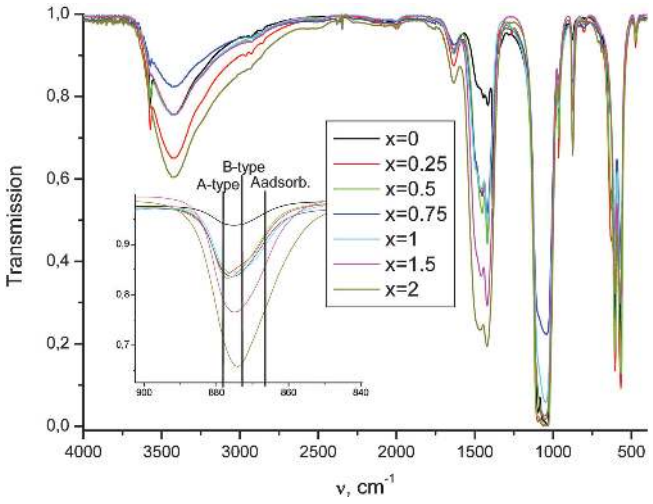

Figure 3. FTIR-spectra for CHAp with various x.

monstrates contraction of the *a*- and expansion of the *c*-axis dimensions. Unfortunately, published data concerning this issue are still controversy, *e.g.* Barralet *et al* [11] reported on maximum in *a* vs carbonate content dependence and opposite behavior for *c*-axis (though the last dependence was only claimed but not presented in the article), while Pieters *et al* [12] did not find any correlation between carbonate content and changing of the lattice parameters. According to the present work, the effect of carbonate content on lattice parameters and cell volumes of the powders under study evaluated with XRD is rather complex (*Fig.2* and table 1). It is possible to separate the following domains along *x*-axis and assign to certain substitution types:

Table 1. Lattice parameters and cell volumes of CHAp sampless ($P6_3/m$), after heat treatment 260 °C/1 hour.

x from $Ca_{10-x}Na_x(PO_4)_{6-x}(CO_3)_x(OH)_2$	a, Å	c, Å	V, Å^3
x = 0	9.402(2)	6.890(1)	527.5(2)
x = 0.25	9.408(2)	6.898(3)	528.7(3)
x = 0.5	9.376(2)	6.893(2)	524.8(2)
x = 0.75	9.355(3)	6.890(2)	522.2(3)
x = 1	9.356(3)	6.889(2)	522.3(3)
x = 1.5	9.335(4)	6.894(3)	520.3(5)
x = 2	9.337(3)	6.904(2)	521.3(2)

1. x=0 – 0.25, featured with a slight expansion of lattice volume and related, presumably, to A-type,
2. x=0.25 – 0.75, transient region revealing noticeable volume contraction of the lattice ($\Delta V/V$=1.2 %); importantly, only for the samples with x=0.25 and 0.5, non-zero values of microstrain, compensated within the bulk of a crystallite, were extracted from XRD profile analysis (ε=0.1 % for both samples, assuming Young modulus for apatite E=100 GPa, it corresponds to density of elastic energy $U_{elast}=0.5E\cdot\varepsilon^2$ =50kJ·m^{-3}); the origin of these contractive microstrains lies in different sizes of CO_3^{2-} and PO_4^{3-} (*i.e.* the reason underlying such a behavior of the lattice in this domain could be a substitution of B-type),
3. x>0.75, with slight contraction of lattice volume, however, without detectable microstrain, that means further filling of B-positions with effective compensation mechanism (relaxation) of substitution strains; possible relaxation channel could be a redistribution of CO_3^{2-} between B- and A-sites, thus, this region seems to correspond to CHAp of AB-type.

The FTIR spectra (*Fig. 3*) showed that all the compositions exhibited the characteristic bands of phosphate groups of the apatite structure at about 550 and 600 cm^{-1} (ν_4), 960 cm^{-1} (ν_1), 1020 – 1120 cm^{-1} (ν_3). The bands at 630 and 3540 cm^{-1} were assigned to OH-groups of the apatite structure. The intensity of these bands decreased as the carbonate content increased.

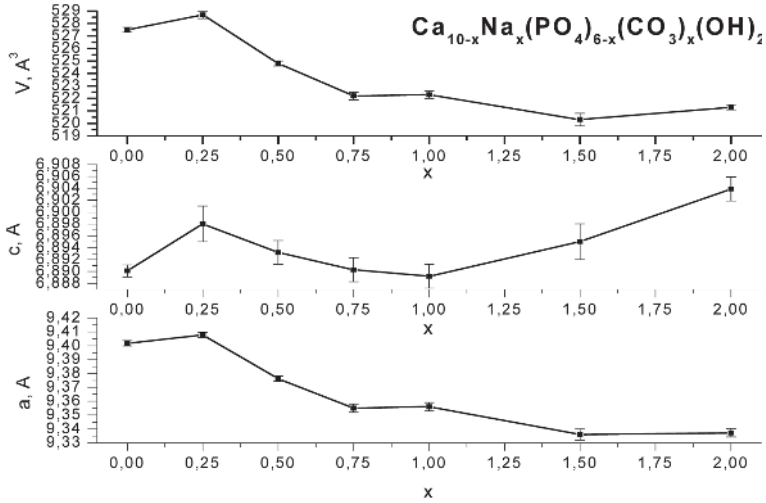

Figure 2. Cell parameters vs. x for CHAp.

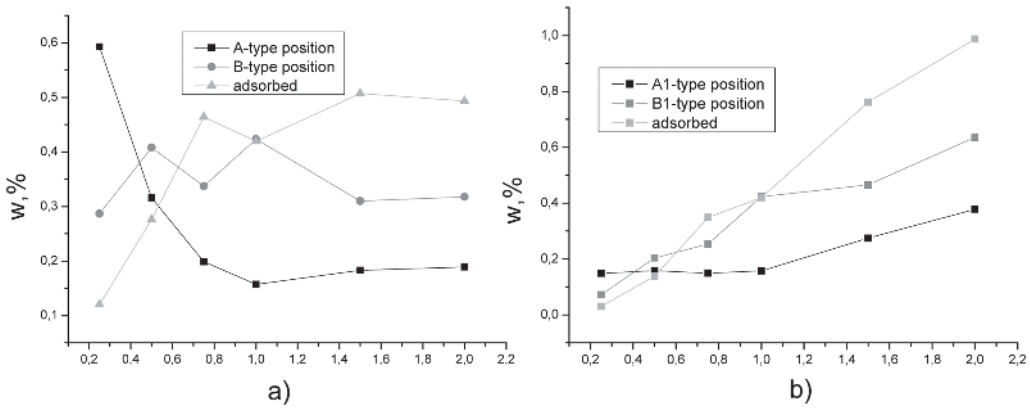

Figure 4. Relationship between varuious forms of carbonate in CHAp a) fraction w of various carbonate forms, and b) absolute content y of carbonate (the sum of y-values for all forms is equal to overall carbonate content x).

Table 2. Weight fraction of CO_3^{2-} in different forms in CHAp

Wt. %	Position A	Position B	Adsorbed CO_3^{2-}
2	18.913	31.759	49.328
1,5	18.284	30.980	50.735
1	15.715	42.335	41.950
0,75	19.856	33.722	46.423
0,5	31.562	40.808	27.630
0,25	59.283	28.685	12.032

The broad bands in the regions 1600–1700 and 3200–3600 cm^{-1} corresponded to adsorbed water. The band at 1380 cm^{-1} was attributed to residual nitrates resulting from synthesis precursors. It was particularly visible in the IR spectrum of the powder that was not washed after synthesis (CHAp, x=1). There are two regions in the spectra which characterize carbonate vibrations: 850–890 cm^{-1} (ν_2 vibrations of carbonate groups), 1400–1650 cm^{-1} (ν_3 vibrations of carbonate groups in apatites). The region of ν_2-type vibrations of carbonate groups is zoomed in fig.3. The shoulders of this band were assigned to carbonate vibrations in A- or B-site of the apatite lattice in accordance with the literature data [1]: 878–880 cm^{-1} to A-type, 871–873 cm^{-1} to B-type, and near 866 cm^{-1} to absorbed CO_3^{2-} (otherwise termed soluble CO_2 [13], or unstable carbonate [14]). We also tried to deconvolute this band peak to three components corresponded to the types of CO_3^{2-} mentioned above, and to quantify their contents in accordance with the areas under the bands obtained as a result of the deconvolution (*Fig.4, table 2*). To the best authors knowledge, this is the first attempt to quantify the type of carbonate ions in CHAp using ν_2-band of CO_3^{2-} in IR-spectra, although, similar fitting of ν_4 phosphate group band by Miller *et al* [15] and OH stretching mode at 3500–3600 cm^{-1} by Veiderma *et al* [16] were done. It is clearly seen from fig.4 a, that a partial contribution of the carbonate of A-type decreses as the index x grows from 0 to 0.75 (domains (a) and (b) according to XRD data), and remains still at x>0.75. At the same time, B-type carbonate oscilates between 30 and 40 %, and adsorbed carbonate has a tendency to grow (Fig.4 a). Absolute contents of all of these species increase with increase of x (Fig.4 b). It is of note that in view of fig.3, the domain (b), termed above as transient state, is featured by increasing of the content of carbonate of B-type at a constant level of A-type doping. This might be the reason for the strain pattern discovered in this domain by the analysis of XRD peak broadening. At x>0.75, both A- and B-type carbonates tend to increase; since they are accompanied by opposite variations of the lattice parameters, microstrains are not revealed within this domain of doping. Thus, all the powders should be considered as AB-type carbonated apatites. The regularities of carbonate substitution deduced from FTIR-spectra agree fairy well with those found with XRD and discussed above.

Coupling XRD, FTIR, microvolumetric data on CO_2 – content and TG/DTA data (the results are summarized in *table 3*), one can try to discriminate between different substitution models. Four models were considered:

A – $Ca_{10}(PO_4)_6(OH)_{2-2x}(CO_3)_x$,

B1 – $Ca_{(10-x)}Na_x(PO_4)_{(6-x)}(CO_3)_x(OH)_2$,

B – $Ca_{(10-x/2)}(PO_4)_{(6-x)}(CO_3)_x(OH)_2$, the model

AB – $Ca_{(10-x)}(PO_4)_{(6-x)}(CO_3)_x(OH)_{2-x}$.

Unfortunately, it is not possible to choose a certain model addressing to this table only. However, it is worth noting that the models of B-type and AB-model fit the data better compared to the model of A-type. The atomic ratio of Ca/P, Na/Ca, CO_3^{2-}/PO_4^{3-} of CHAp sample were calculated from the results of chemical analysis. *Fig. 5* (a) shows that there is insignificant incorporation of Na into the crystal structure. In order to get more information on substitution mechanism (*viz.* charge compensation in the course of aliovalent doping), experimental plot of Ca/P vs CO_3^{2-}/PO_4^{3-} was compared with two models discussed above (Fig.5 b):

1. model B related to the quasi-chemical equation
   $Ca^{2+} + 2PO_4^{3-} = V_{Ca} + 2CO_3^{2-}$, and to the formula
   $Ca_{(10-x/2)}(PO_4)_{(6-x)}(CO_3)_x(OH)_2$;
2. model A related to the quasi-chemical equation
   $2OH^- = V_{OH} + CO_3^{2-}$, and to the formula
   $Ca_{10}(PO_4)_6(OH)_{2-2x}(CO_3)_x$.

The slope of the experimental plot matches well the model B in the region x>0.75. Thus, chemical analysis confirms the substitution scenario made on the basis of structural techniques (see above). The molecular formula of the samples was derived from both structural and analytical data. Two points are essential for deriving the formula: (i=1) independent filling of A- and B-postions accompanied by formation of vacancies in OH- and Ca-sites, respectively, and (ii=2) redistribution of the dopant between A- and B-sites evoking relaxation of the lattice from substitution stresses. Thus, CHAp of AB-type (assuming insignificant incorporation of Na) could be presented as:

Table 3. Content of CO_3^{2-} (wt.%) in CHAp in comparison with theoretical values in different substitution models: A - $Ca_{10}(PO_4)_6(OH)_{2-2x}(CO_3)_x$, B - $Ca_{(10-x/2)}(PO_4)_{(6-x)}(CO_3)_x(OH)_2$, B1 - $Ca_{(10-x)}Na_x(PO_4)_{(6-x)}(CO_3)_x(OH)_2$, AB - $Ca_{(10-x)}(PO_4)_{(6-x)}(CO_3)_x(OH)_{2-x}$.

x	% CO_3^{2-} Micro volumetric	%(CO_2+H_2O) TG (±0.5)	Model A		Model B		Model B1		Model AB	
			CO_3^{2-}, %	(CO_2+H_2O), %	CO_3^{2-}, %	(CO_2+H_2O), %	CO_3^{2-}, %	(CO_2+H_2O), %	CO_3^{2-}, %	(CO_2+H_2O), %
0	1,5±0,05	3.4	0	1.79	0	1.79	0	1.79	0	1.79
0.25	3,8±0,15	3.2	1.48	2.42	1.51	2.93	1.51	2.92	1.53	2.73
0.5	3,86±0,24	–	2.95	3.05	3.07	4.09	3.07	4.09	3.13	3.70
0.75	6,09±0,40	6.3	4.39	3.66	4.67	5.29	4.66	5.28	4.81	4.73
1	7,1±0,33	6.5	5.82	4.27	6.32	6.53	6.30	6.51	6.58	5.81
1.5	9,67±0,61	8.9	8.63	5.46	9.76	9.11	9.72	9.07	10.39	8.14
2	13,36±0,02	10.9	11.36	6.63	13.42	11.85	13.33	11.77	14.63	10.73

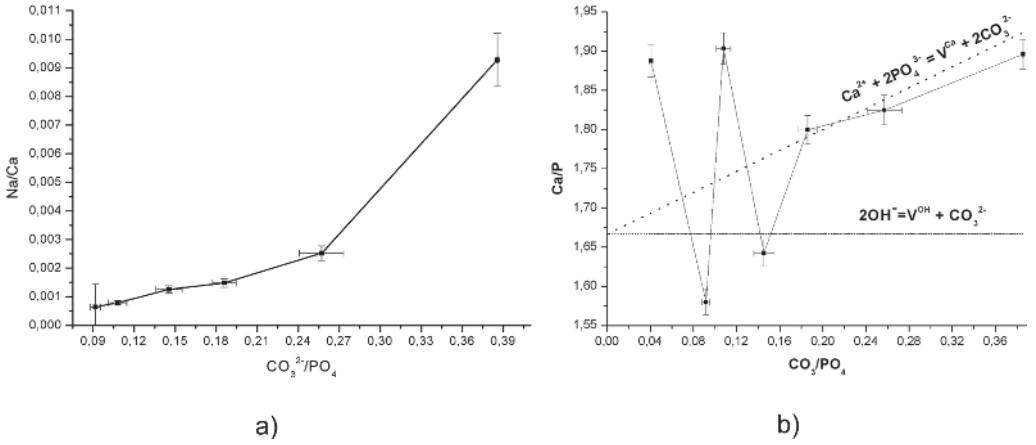

Figure 5. a) Chemical composition of CHAp: CO_3^{2-}/PO_4^{3-} vs. Na/Ca, b) experimental plot of Ca/P vs CO_3^{2-}/PO_4^{3-} in comparison with two substitution models.

$(Ca_{10-xu/2}V_{xu/2})\{(PO_4)_{6-xu}(CO_3)_{xu}\}[(OH)_{2(1+yu-y)}(CO_3)_{y(1-u)}V_{y(1-u)}]$,

where ( ) – positions of Ca, { } stands for positions of B-type, [ ] – for positions of A-type, V denotes a vacancy, parameter $0 < x < 6$ reflects occupancy of B-type positions, and parameter $0 < y < 1$ does the same for A-type, parameter $0 < u < 1$ describes a transition between B- and A-positions alike a well-known parameter of inversion for a spinel structure.

Transmission electron microscopy (TEM) observations showed the powders with CHAp crystals less than 100 nm, agglomerated into bigger particles. Switching of particle shape from a needle-like to a spherical one is situated as the carbonate content increases. It is of note that in some cases (for intermediate values of *x*) it was possible to observe two different types of morphology within the same sample. We believe that this fact is an indication of a non-uniform distribution of carbonate ions over the samples, coming from variation of the composition across a reaction vessel. Another TEM-observation, neither consisted with available literature, was well-resolved mesoporosity of the samples varied non-monotonously with *x* (*Fig. 6*). The pores filled with a mother solution can be decrypted at 500–800 °C according to TG/DTA (*Fig. 7*). Let us underline here that the sizes of crystallites deduced from XRD profile analysis were systematically lower compared to dimensions determined by TEM, yet another feature consisted in that XRD crystallite sizes (for both [001] and [100] directions) decreased with increase of *x*, however, non-monotonously, with a local maximum around *x*=0.5–0.75). Just the opposite behavior demonstrated variation of specific surface values with *x*. Bearing in mind the distinct mesoporosity of the samples, it becomes clear that the crystallite sizes obtained from XRD line broadening (or the volumes of coherent scattering) refer more to interpore distance than to overall dimensions of a mesoporous body. Apparently, this distance is maximal for the samples from the transient region with *x*=0.25–0.75, and, hence, the porosity of these samples is minimal. Being the most bulky, these samples concentrates substitution stresses in a greater extent compared to other holey samples, this conclusion is consistent with the observation of the trend of the lattice parameters. The (mean over the sample) vales of lattice parameters reflect a distribution of the dopant across the crystals, the sizes of crystals and their porosity, which undoubtedly depend on conditions of synthesis (temperature, pH, ripening time).Thus, the discrepancy in the trends of CHA lattice parameters presented by different authors with increase of carbonate content becomes clear.

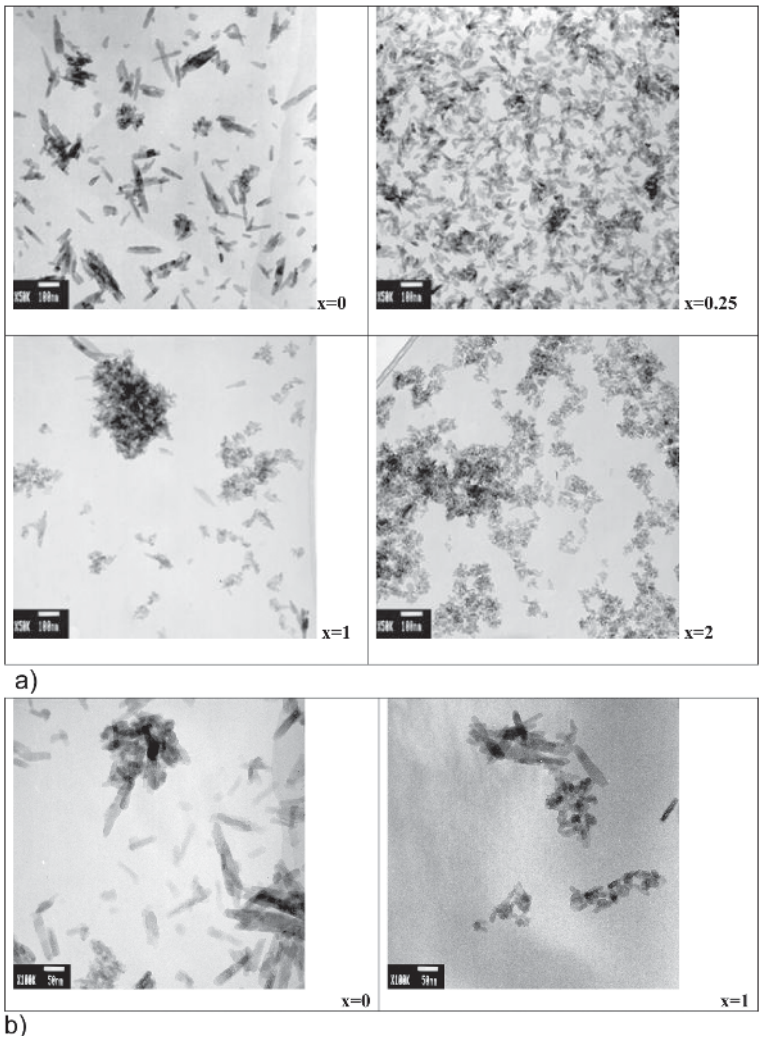

Figure 6. TEM image of CHAp powders a) with x=0, 0.25, 1, 2, and b) enlarged view for the samples with x=0 and 1.

Bioactivity of the samples was evaluated *in vitro* using two kinds of experiments: 1) dissolution in acetic media simulating active resorption with osteoclastic cells, and 2) dissolution-precipitation phenomena in SBF solutions at near physiological pH values representing the activity of the material with respect to blood plasma.

A correlation between dissolution rate of CHAp in acetic buffer and microstrain/size of crystals was revealed (*Fig. 8*). It is worth noting that specific dissolution rate (normalized to unit surface) demonstrated quite a sharp gain around the point of substitution mechanism changing (x=0.25–0.75); this area was featured also with pronounced microstrains (ca. 0.1 %) found in CHAp nanocrystals as it was stated by XRD profile

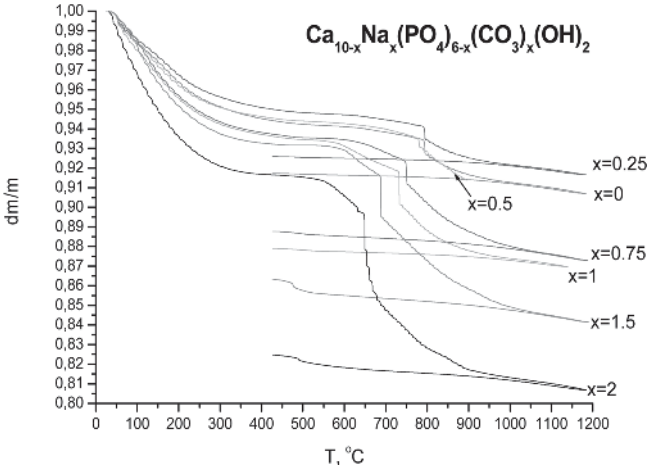

Figure 7. TG of CHAp powders (quasi-isothermal mode).

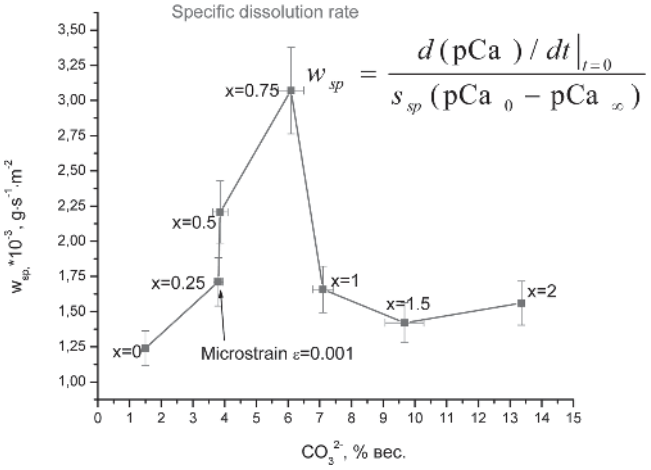

Figure 8. Dissolution rate of CHAp in acetic buffer solution.

analysis. It was shown above that these microstrains correspond to $U_{elast} \approx 50 kJ \cdot m^{-3}$ (or, assuming density of CHAp $\approx 3\ g \cdot cm^{-3}$ [13], to $\approx 0.02\ kJ \cdot mol^{-1}$). This contribution to overall energy balance of a crystal looks quite subtle, however, it really influences in dissolution rate. Then, we have to conclude that this elastic energy is accumulated in the volume less than the volume of a crystallite (and this is consistent with the nature of microstrains causing X-ray line broadening; corresponding stresses are to be balanced within the volume of a crystallite), and the reason for it can be non-uniform distribution of the dopant across the crystal coming from non-equilibrium conditions of synthesis. This subject was extensively discussed with respect to the composition of distorted surface layer in biogenic apatite nanocrystals (see, *e.g.* [17]). As to overall dissolution rate (not normalized to unit surface), it grows with the increase of the carbonate content.

The dissolution-precipitation of CHAp under physiological pH was evaluated *in vitro* using SBF media. Samples were soaked in SBF for different time intervals (from 7 to 21 days) at 37 °C and pH 7.4. Afterward, they were examined with SEM to analyze a fresh apatite layer precipitated from SBF. It is quite clear from *fig. 9* (a), that formation of the apatite layer on the surface of the materials is observed. After 7 days of immersion in SBF the surface of bioactive material was covered by open-work layer consisting of plate like self-organized particles of newly formed carbonate apatite (Fig. 9. b). This layer becomes thicker as the carbonate content in CHp increases.

The powders under study were prepared for co-culturing with human fibroblasts *in vitro* and to fill model defects in a small laboratory animal (Vistar rat). This issue will be addressed in details in a forthcoming paper. However, it is important to draw a preliminary conclusion on *in vitro* and *in vivo* behavior of the samples in order to validate the results of the dissolution and the precipitation experiments described above. *In vitro* fibroblast cell test shows that after 3 weeks of co-culturing there was observed cell adhesion to the surface of the CHAp powders. Primary growth and proliferation of fibroblasts attached to agglomerates of the nanopowders took place. No one dead cell was detected, so the materials are non-cytotoxic. After the cell tests, granular CHAp material (size fraction of 300 – 500 mkm) was implanted into the condyle of a Vistar rat. Two weeks later a bone capsule formed around the granules and an active ingrowth of *de novo* bone trabecules between remained deposits occured. Study of histological sections revealed that resorption of the implant and its ossification accelerated with increase of the carbonate content.

Finally, growth of carbonate content in CHAp gives rise to defects of the crystal lattice and specific patterns of microstructure; of these, there are vacancies in Ca- and OH-sublattice, non-uniform distribution of the dopant across the crystal volume, distinct mesoporosity of the crystals. Accumulation of these defects leads to higher solubility of CHAp crystals and, thus, to better bioactivity.

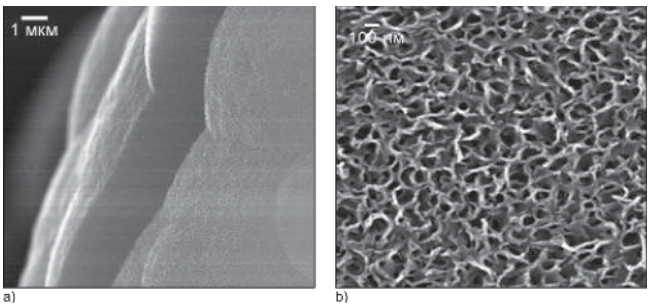

Figure 9. CHAp samples after 21 days, 37 °C in SBF, pH = 7.4: a) lateral surface of chip; b) top surface layer.

4 Conclusions

Incorporation of carbonate ions into the structure of apatite leads to the formation of point defects (vacancies) in Ca- and OH-sublattices as well as to microstrains revealed in CHAp nanocrystals by XRD technique. The reason of this strain pattern consists in mechanical stresses coming from differences of ionic radii of the dopant and substituted specie and/or inhomogeneous distribution of the dopant in the vicinity of the surface of the nanocrystals. These peculiarities of the real structure of CHAp nanocrystals in conjunction with a prominent decrease of the sizes of the crystals while the carbonate content grows, contribute to an increase of free energy of the crystals, thus providing better solubility and resorption.

It was shown that there is insignificant incorporation of Na into the crystal structure of HAp. Over the range of 0 – 4 % wt. ($x < 0.25$), the substitution of OH- by CO_3^{2-} takes place leading to A-Type of CHAp, further increase of CO_3^{2-}-content enhances PO_4^{3-}-substitution giving AB-type of CHAp. It is of importance that redistribution of the carbonate between the two sites could provide a channel for the lattice relaxation from stresses coming with the CO_3^{2-}/ PO_4^{3-}/OH substitution, and, therefore, to decrease the level of microstrains in the crystal of CHAp.

Higher dissolution rate of CHAp powders (in comparison with pure HAp) was observed during the experiments in buffered solutions at pH = 5.5 and in SBF. The increase of the dissolution rate can be related to intrinsic microstrains of HAp crystals due to significant difference in effective ionic radii of carbonate and phosphate groups.

According to *in vitro* solubility test, the bioactivity of the samples is increasing with the growth of carbonate content due to accumulation of the defects in CHAp nanocrystals. *In vitro* and *in vivo* experiments, aimed at an assessment of CHAp ability to interact with cultured cells or tissues, demonstrated that the increase of carbonate ion content in HAp structure improves CHAp resorption and enhances its osteointegration.

5 Acknowledgements

The work was partially supported by RFBR grants 07 – 08 – 00576, 09 – 03 – 01078 and Federal Program "R&D in priority directions of science and technology in Russia for the period of 2007 – 2012 years" (state contract 02.513.12.3008).

The authors gratefully acknowledge the contribution of Dr. I.V. Fadeeva, Dr.V.S. Komlev in helping the materials preparation and Prof. M.L. Semenova, Prof. L.V.Belousov, S.A. Sergeev, Dr. A.N. Gurin in providing the biomedical experiments.

6 References

1. J.P. Lafon, E. Champion and D. Bernache-Assollant, *J. Eur. Cer. Soc.* **2008**, *28*, 13947.
2. R.Z. LeGeros, *Clin. Orthoped. rel. Res.* **2002**, *395*, 81.
3. I.R. Gibson, W. Bonfield, *J. Biomed. Mater. Res*. **2002**, *59*, 697.
4. L.G. Ellies, D.G.A. Nelson and J.D.B. Featherstone, *J. Biomed. Mater. Res*. **1988**, *22*, 137.
5. A. Ito, K. Maekawa, S. Tsutsumi, F. Ikazaki and T. Tateishi, *J. Biomed. Mater. Res*. **1997**, *36*, 522.
6. M. Vignoles, G. Bonel, D.W. Holcomb, R.A. Young, *Calcif. Tissue. Int*. **1988**, *43*, 33.
7. F.C.M. Driessens, *Ph.D. Thesis*, Edinburgh University, UK, **1995**.
8. T. De Keijser, J.I. Langford, E.J. Mittemeijer, A.B.P.Vogels, *J. Appl. Cryst*.**1982**,*15*, 3087.
9. S.E. Dahlgren. *Z. analyt. Chem*. **1962**, *189,* 243.
10. T. Kokubo, H. Kushitani, S. Sakka, T. Kitsugi, Y. Yamamuro, *J. Biomed. Mater. Res.* **1990**, *24*, 721.
11. J. Barralet, S. Best, W. Bonfield, *J. Biomed. Mater. Res.* **1998**, *41*, 79.
12. I.Y. Pieters, E.A.P. De Maeyer, R.M.H. Verbeeck, *Inorg. Chem*. **1996**, *35*, 5791.
13. R.N. Panda, M.F. Hsieh, R.J. Chung, T.S. Chun*, J. Phys. Chem. Solids*, **2003**, *64*, 193.
14. C. Rey, B. Collins, T. Goehl, I.R. Dickson, M.J. Glimcher, *Calcif. Tissue Int*. **1989**, *45*, 157.
15. L.M. Miller, V. Vairavamurthy, M.R. Chance, R. Mendelsohn, E. P. Paschalis, F. Betts, A.L. Boskey, *Biochim. et Biophys. Acta*. **2001**, *1527*, 11.
16. M. Veiderma, K. Tõnsuaadu, R. Knubovets, M. Peld, *J. Organometal. Chem*. **2005**, *690(10)*, 2638.
17. T. Kanazawa, *Inorganic phosphate materials*, Elsevier Science Publishing B.V., Amsterdam **1989**.
18. J.D. Pasteris, B. Wopenka, J.J. Freeman, K. Rogers, E, Valsami-Jones, J.A.M. van der Houwen, M.J. Silva, *Biomat*. **2004**, *25*, 229.

Correspondence author: Valery I. Putlayev*,* Department of Materials Science, Moscow State University, 119991, Moscow, Russia, E-mail: putl@inorg.chem.msu.ru

Received in final form: November 3, 2008 [T 383]